



Changes in planktic and benthic foraminifer assemblages in the Gulf of Lions, off south France: Response to climate and sea level change from MIS 6 to MIS 11

Aleix Cortina, Francisco Javier Sierro, and José Abel Flores

*Department of Geology, University of Salamanca, Plaza de la Merced sn, 37008, Salamanca, Spain
(acortina@usal.es)*

Gabriel Filippelli

*Department of Earth Sciences, Indiana University-Purdue University at Indianapolis (IUPUI),
Indianapolis, Indiana, USA*

Serge Berné

CEFREM, Université de Perpignan, 66860, Perpignan, France

[1] A multidisciplinary study involving micropaleontological and geochemical tools was carried out in borehole PRGL1 (Promess 1), with the aim of reconstructing the impact of climate change and sea level variation between 133 ka and 406 ka in the upper slope of the Gulf of Lions. We used factor analysis to obtain three main benthic assemblages related to eutrophic, mesotrophic, and oxygenated environments; planktic foraminifers were grouped as warm-water and cold-turbulent species. These results were compared with records of CaCO₃ and major and trace elements (Al, Ca, K, Sr) as well as the C/N ratio of organic matter. Power and cross-spectral analysis showed a straightforward relationship between precession minima and thermal stratification of the water column as well as the occurrence of eutrophic bottom conditions during lowstand periods and mesotrophic environments at times of highstand. These eutrophic-mesotrophic oscillations, usually driven by global eustatic change, also involved regional variations in CaCO₃ source to this environment. During periods of precession maxima, enhancement of northwesterly winds increased primary productivity by mixing, enhancing the percentage of cold-turbulent species in the water column and the proportion of oxygenated benthic species on the bottom. During interglacial stages, these events were recorded by lower biogenic carbonate at the expense of higher silicate-related components most likely due to a higher supply from Pyrenees rivers. The record of oxygenated benthic species can be a good proxy to monitor past changes in Winter Intermediate Water dynamics driven by northwesterly winds.

Components: 9,900 words 7 figures, 4 tables.

Keywords: foraminifer; sea level; northwesterly winds; Gulf of Lions.

Index Terms: 3344 Atmospheric Processes: Paleoclimatology (0473, 4900); 3030 Marine Geology and Geophysics: Micropaleontology (0459, 4944); 1051 Geochemistry: Sedimentary geochemistry.

Received 5 July 2012; **Revised** 12 February 2013; **Accepted** 12 February 2013; **Published** 30 April 2013.

Cortina, A., F. J. Sierro, G. Filippelli, J. A. Flores, and S. Berné (2013), Changes in planktic and benthic foraminifer assemblages in the Gulf of Lions, off south France: Response to climate and sea level change from MIS 6 to MIS 11, *Geochem. Geophys. Geosyst.*, 14, 1258–1276, doi:10.1002/ggge.20096.

1. Introduction

[2] The Gulf of Lions plays an important role in the general circulation of the Mediterranean Sea, since it is the source of Western Mediterranean Deep Water (WMDW), as well as the Winter Intermediate Water (WIW). These water masses are formed when Modified Atlantic Water cools and sinks to deep or intermediate depths, respectively [Millot, 1999]. Several paleoceanographic studies have highlighted the importance of past climate changes on the variability of the WMDW and circulation dynamics of western Mediterranean [Cacho *et al.*, 2000; Sierro *et al.*, 2005; Frigola *et al.*, 2008] but little is known about past WIW dynamics.

[3] The location of the core PRGL1 on the upper slope of the Gulf of Lions has proven suitable to monitor past variations in sea level [Sierro *et al.*, 2009], as a consequence of the differential river Rhone input between highstands (low input) and lowstands (high input). The position of this site is excellent for monitoring past variability of WIW and Dense Water Shelf Cascading (DWSC), as it is situated in a zone of moderate benthic energy compared to zones of extreme benthic energy around the Cap de Creus and Lacaze-Duthiers canyon heads further to the west. This was demonstrated by measurements in the nearby Bourcart (Aude) canyon head, where current velocities at 300 m water depth were on the order of 0.4 m/s during winter 2003–2004 [Gaudin *et al.*, 2006]. DWSC is produced during winters when dry and cool northwesterly wind events are prolonged and surface waters on the continental shelf become denser and sink [Canals *et al.*, 2006; Palanques *et al.*, 2006]. Dense waters flow down the continental slope until they reach their hydrostatic equilibrium level contributing to the formation of WIW [Dufau-Julliand *et al.*, 2004] and even to renewal of deep waters in the Mediterranean basin [Béthoux *et al.*, 2002; Canals *et al.*, 2006]. Consequently, the study of the past ventilation dynamics on the upper slope is important to record the contribution of the continental shelf to WIW and WMDW. Moreover, it will contribute to understanding the variability of WMDW, since northwesterly winds drive changes in this water mass [Cacho *et al.*, 2000; Moreno *et al.*, 2002; Sierro *et al.*, 2005].

[4] Our previous work at the same core site was focused on the relationship between planktic and benthic foraminifer assemblages during MIS 6 and 7, and how they were linked to changes in the intensity of the northwesterly winds and sea level oscillations [Cortina *et al.*, 2011]. Sea level

oscillations were mainly monitored by benthic foraminifer assemblages adapted to either eutrophic (low sea level) or mesotrophic (high sea level) environments as a consequence of the different position of Rhone river mouth. Benthic foraminifer assemblages also responded to bottom oxygenation episodes as demonstrated by the occurrence of species adapted to more oxygenated conditions. These ventilation episodes were linked to an intensification of the northwesterly winds. In this work, we extend this study to MIS11 and use other geochemical proxies such as C/N ratio in organic matter (considered a proxy of the source of organic matter), calcium carbonate (CaCO₃), *Globigerina bulloides* $\delta^{18}\text{O}$ record, and major and trace elements (Al, Ca, K, Sr). This study aims to: (1) understand the relationship between glacial-interglacial changes in benthic and planktic fauna and marine sediment composition, and (2) determine how these changes were linked to changes in sea level and ventilation of intermediate waters of the NW Mediterranean.

2. Regional Setting

[5] The Gulf of Lions is situated at the northwestern part of the Mediterranean Sea. The general circulation is mainly driven by the Northern Current, which is divided in two branches: the principal branch flowing through the open sea along the Catalano-Balearic Sea and the secondary branch that circulates along the continental shelf edge [Millot, 1990] (Figure 1).

[6] Unlike the general oligotrophic character of the Mediterranean Sea, the Gulf of Lions is relatively eutrophic due to its particular hydrodynamic conditions. Fertility is mainly induced by winter vertical mixing, upwelling events, and the nutrient influence of River Rhone [Lefèvre *et al.*, 1997]. The study site is situated southwest of the Rhone delta, where about half of the total biological productivity is driven by riverine input of nutrients [Lefèvre *et al.*, 1997].

3. Material and Methods

[7] We studied borehole PRGL1, drilled during the Promess1 campaign (summer 2004) in the Gulf of Lions (42.690 N, 3.838 E) (Figure 1) on the interfluvial of the Boucart and Herault canyons at a water depth of 298 m. The location of this site is near the shelf break, making it ideal for recording past changes in Rhone supply as well as productivity

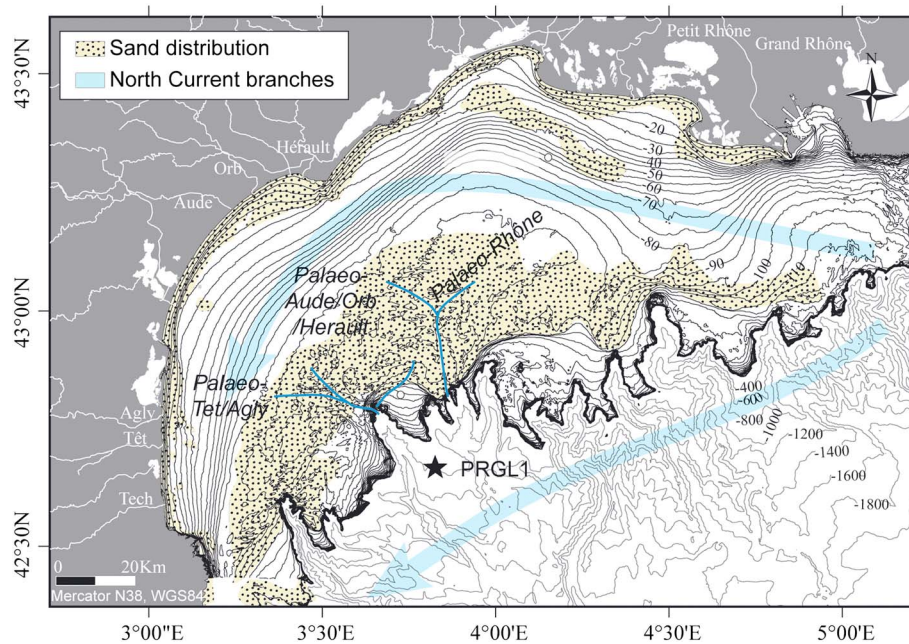


Figure 1. Map of the Gulf of Lions taken from *Jouet et al.* [2006]. The present-day morphology and the sand distribution on the continental shelf [*Aloisi*, 1986] illustrating the last deglacial sea-level rise. Blue arrows represent the two North Current branches. Core site PRGL1 is represented by a black star.

and ventilation in the upper part of the water column (its paleodepth at glacial times was about 150 m).

[8] In the laboratory, 1 cm thick slices were taken every 10 cm. In this study, we analyzed samples from 73.5 to 199.115 mbsf (meter below sea floor) (133 ka to 406 ka) corresponding to Marine Isotope Stages (MIS) 6 to 11.

3.1. Age Model and *G. bulloides* $\delta^{18}\text{O}$ Record

[9] The age model was based on *Sierro et al.* [2009] and *Frigola et al.* [2012]. From 73.5 to 157.10 mbsf, we used the age model published by *Sierro et al.* [2009]. For the second interval (from 157.10 to 199.115 mbsf), we used the age model published by *Frigola et al.* [2012]. In both cases, the age model was mainly based on comparison of the *G. bulloides* $\delta^{18}\text{O}$ record with the LR04 benthic stack [*Lisiecki and Raymo*, 2005]. The calculated sedimentation rates resulted in an average sampling resolution of 1150 yr during interglacials and 160 yr during glacial stages.

3.2. Benthic and Planktic Foraminifer Assemblages

[10] A subsample of approximately 15 g was taken, dried in an oven, and weighed. Each subsample was

washed over a sieve with 150 μm mesh to remove the smaller fraction. The size fraction larger than 150 μm was used for counting benthic and planktic foraminifers. The samples were split up until at least 300 individuals of benthic foraminifers and 400 of planktic foraminifers were counted. This goal could not be achieved in planktic foraminifers in all samples, especially in glacial periods due to their scarcity at times of higher sedimentation rates. Consequently, for the quantitative study, we only took into account samples with more than 100 individuals that may be enough to work with species with a relative proportion of at least 5% of the assemblage [*Fatela and Taborda*, 2002]. The samples counted at the present study comprise from MIS 8 to 11, whilst samples from MIS 6 and 7 were taken from a previous study [*Cortina et al.*, 2011]

[11] Taxonomy of benthic foraminifers was based on *Loeblich and Tappan* [1988]. Subsequently, a total of 129 species were recognized using *Ellis and Messina* [2007]. We did not separate *Bulimina marginata* and *Bulimina aculeata* species because intergrading of both did not always allow their distinction [*Filipsson et al.*, 2010]. In fact, some authors consider both types to be the same species (e.g., *B. marginata* var. *marginata* and *B. marginata* var. *aculeata*) [*Jorissen*, 1987]. Therefore, we referred our results on these species as *B. aculeata*

/ *B. marginata* complex. Planktic foraminifers were identified on the basis of the taxonomic classifications of *Hemleben et al.* [1989].

[12] In order to simplify the high amount of variables in benthic foraminifer, we applied an R-mode Principal Component Analysis performed by STATISTICA (StatSoft, Inc, version 7, 2004). We note that the statistical distributions of the benthic foraminifer assemblages were not normal but log-normal. Consequently, to improve correlations between variables when a Principal Component Analysis was performed, a $\log_{10}(x+1)$ transform was applied, where x is percentage data, and we sum 1 as logarithm of 0 cannot be computed. Besides, normalizing the data, this transformation increased the importance in our analysis of the species that were less abundant.

3.3. Geochemical Data

3.3.1. C/N Ratio of Organic Matter and Calcium Carbonate

[13] To obtain the C/N ratio of organic carbon, inorganic carbon was first removed following standard procedures [*van Iperen and Helder*, 1985], although HCl concentrations were increased from 1N to 2N to completely remove carbonate [*Kennedy et al.*, 2005]. We added 10 ml of 2N HCl to approximately 200 mg of crushed sample in 50 ml centrifuge tubes. The samples were dried overnight at $\sim 70^{\circ}\text{C}$ to evaporate water and excess HCl. In order to ensure all HCl was removed, samples were rinsed with deionized water, centrifuged for 10 min at 8000 r.p.m., and the supernatant was decanted—this step was repeated twice. After the second DI rinse, wet sediment was transferred to a vial and oven dried at 65°C until all the water was evaporated. Samples were then analyzed with a Flash EA 1112 Elemental Analyzer to obtain the percentage weight of organic carbon (%OC*) and nitrogen (%N*) on a carbonate-free basis. The C/N ratio was determined from percentage of total nitrogen (%N), measured over samples without treatment, and percentage of total organic carbon (%OC) calculated from %OC*.

[14] In order to calculate percent calcium carbonate (%CaCO₃) we used inorganic carbon (%IC) by multiplying 100/12 (ratio weight CaCO₃/C). To measure %IC, we ran crushed samples at CHN analyzer to obtain percentage of total carbon (%TC). With %TC and %OC*, it was possible to infer %IC and %OC. We have two unknown variables, so it is necessary to construct a double linear equation system as follows:

$$\%TC = \%IC + \%OC$$

$$\%OC = (\%OC^* / (100 - (\%IC * 100/12))) * 100$$

[15] Solving these two equations, we obtained %OC and %IC.

3.3.2. Elemental Analysis

[16] For total digestions, ~ 0.1 g of each sample was dissolved using a MDS 2000 Microwave Digestion System and concentrated trace metal grade HNO₃, HF and HCL following EPA SW846 Method 3051. After the digestion was complete, we added boric acid to stabilize the solutions. The samples were transferred to new 50 ml polypropylene centrifuge tubes and diluted to 50 ml Milli-Q water. To determine total elemental concentrations a PerkinElmer iCAP 6000 Inductively Coupled Plasma-Optical Emission Spectrometer, with a high speed, high-resolution double monochromator with a CCD array detector was used. From measured concentrations, we calculated percentages of Al, Ca, K, and Sr using standardization via standard solutions. Typical reproducibility of replicates is less than 2% for these elements.

3.3.3. Biogenic Carbonate Index

[17] To estimate the main calcium carbonate sources in the Gulf of Lions, we used the biogenic carbonate index. To calculate this index, both variables were standardized following this procedure. Given a value x , we obtain its standardized value ($x_{\text{standardized}}$):

$$x_{\text{standardized}} = (x - \mu) / \sigma;$$

μ : mean of the variable

σ : standard deviation of the variable

[18] The biogenic carbonate index was then calculated by subtracting the standardized CaCO₃ value from the standardized Sr value (Sr-CaCO₃). Lower values are related to larger positive deviations of CaCO₃ content (from its mean) and/or negative deviations of Sr from its mean. Lower values in this index were linked to higher input rates of carbonate relative to Sr, and higher values were linked to lower carbonate supply relative to Sr.

Table 1. Comparison Between Main Species of Benthic Foraminifer Factors Extracted by R-mode Principal Component in the Present Study and Those From Cortina et al. [2011]. In Bold Are Highlighted Common Species

[Cortina et al., 2011]																	
Factor 1			Factor 2			Factor 3			Factor 1B (mesotrophic)			Factor 2B (oxygenated)			Factor 3B (eutrophic)		
Explained variance = 42.5%			Explained variance = 18.1%			Explained variance = 20.6%			Explained variance = 38.7%			Explained variance = 16.3%			Explained variance = 25.1%		
Species	Factor scores	Species	Factor scores	Species	Factor scores	Species	Factor scores	Species	Factor scores	Species	Factor scores	Species	Factor scores	Species	Factor scores		
<i>B. aculeata</i> /	4.54872	<i>Trifarina angulosa</i>	5.58156	<i>Brizalina dilatata</i>	8.84495	<i>Melonis barleeanum</i>	3.91684	<i>Trifarina angulosa</i>	4.44388	<i>Brizalina dilatata</i>	7.05786						
<i>B. marginata</i>	3.82807	<i>Cassidulina laevigata</i>	5.0284	<i>B. aculeata</i> /	4.18673	<i>Uvigerina peregrina</i>	3.53463	<i>Cassidulina laevigata</i>	3.99755	<i>Bulimina marginata</i>	5.03226						
<i>Cibicides</i>	3.75732	<i>Quinqueloculina seminulum</i>	4.14785	<i>B. marginata</i>	2.55524	<i>Cibicides laevigata</i>	3.17650	<i>Quinqueloculina seminulum</i>	3.75286	<i>Bulimina marginata</i>	3.74731						
<i>pachyderma</i>	3.63111	<i>Pyrgo oblonga</i>	3.18345	<i>Cassidulina laevigata</i>	2.26286	<i>pachyderma</i>	3.15283	<i>Miliolinella subrotunda</i>	3.22584	<i>aculeata</i>	2.95620						
<i>barleeanum</i>	3.06163	<i>Miliolinella subrotunda</i>	2.6226	<i>Uvigerina peregrina</i>	1.52543	<i>Bulimina inflata</i>	2.85459	<i>Miliolinella subrotunda</i>	3.06149	<i>Cassidulina laevigata</i>	1.59493						
<i>Bulimina inflata</i>	3.03441	<i>Lobatula lobatula</i>	2.54567	<i>Sphaeroidina bulloides</i>	1.50105	<i>Cassidulina laevigata</i>	2.68140	<i>Pyrgo oblonga</i>	2.62957	<i>Cibicidina foltorum</i>	1.41555						
<i>Cassidulina laevigata</i>	2.76511	<i>Cibicidina foltorum</i>	2.31935	<i>Quinqueloculina seminulum</i>	1.11372	<i>Bulimina marginata</i>	2.66617	<i>Lobatula lobatula</i>	2.45404	<i>Lobatula lobatula</i>							
<i>Uvigerina peregrina</i>	2.48833	<i>Astronomion stelligerum</i>	1.86608	<i>Gavelinopsis praegeri</i>	1.05007	<i>Trifarina angulosa</i>	2.56960	<i>Gavelinopsis praegeri</i>	1.37728	<i>Gavelinopsis praegeri</i>							
<i>Globocassidulina subglobosa</i>	2.02608	<i>Miliolinella sp4</i>	1.08962	<i>Miliolinella subrotunda</i>		<i>Globocassidulina subglobosa</i>	1.93571	<i>Astronomion stelligerum</i>	1.34720	<i>Astronomion stelligerum</i>							
<i>Textularia articulata</i>	1.6046					<i>Textularia articulata</i>	1.65548	<i>Brizalina dilatata</i>	1.12819	<i>Brizalina dilatata</i>							
<i>Trifarina angulosa</i>	1.45094					<i>Planulina ariminensis</i>	1.61935	<i>Bulimina aculeata</i>	1.09950	<i>Triloculina tricarinata</i>							
<i>Planulina ariminensis</i>	1.30016					<i>Bulimina aculeata</i>	1.57641	<i>Sigmoilopsis schlumbergeri</i>	1.07760	<i>Miliolinella sp4</i>							
<i>Brizalina alata</i>	1.06289					<i>Sigmoilopsis schlumbergeri</i>	1.45113	<i>Brizalina alata</i>	1.03190	<i>Pullenia quadriloba</i>							
<i>Sigmoilopsis schlumbergeri</i>						<i>Gyroidina neosoldanii</i>											

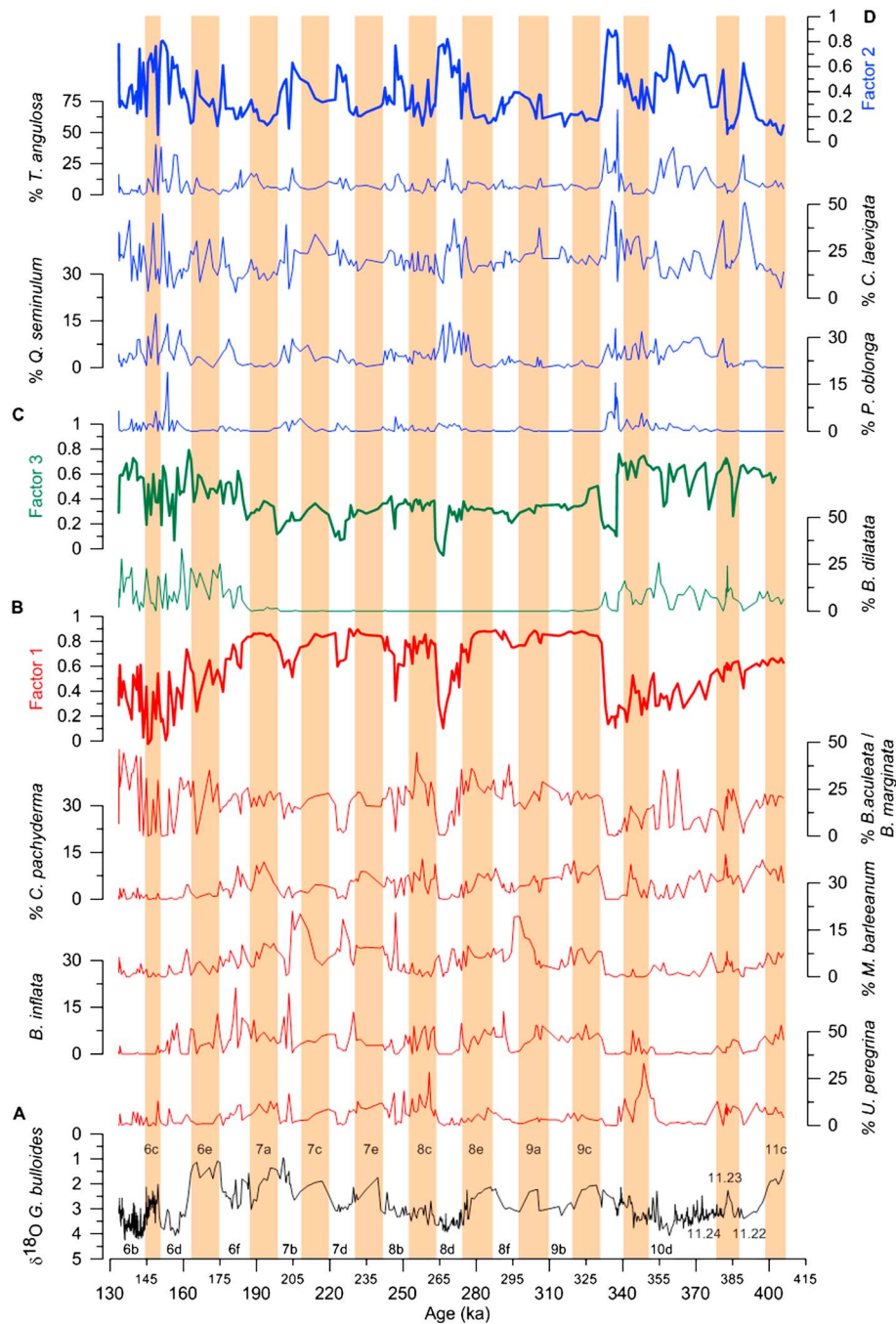


Figure 2. Benthic foraminiferal assemblages at PRGL1. A. *G. bulloides* $\delta^{18}\text{O}$ values. The values from 133 ka to 265 ka were taken from *Sierro et al.* [2009], while values from 266 ka to 406 ka were taken from *Frigola et al.* [2012]. B. Factor 1 loadings and the percentages of its most important species: *B. aculeata* / *B. marginata*, *C. pachyderma*, *M. barleeanum*, *B. inflata*, and *U. peregrina*. C. Factor 3 loadings and the percentages of its most important species: *B. dilatata*. D. Factor 2 loadings and the percentages of its most important species: *T. angulosa*, *C. laevigata*, *Q. seminulum*, and *P. oblonga*. Orange bars represent warming events interpreted on the basis of $\delta^{18}\text{O}$ values of *G. bulloides* and % warm-water planktic species.

3.4. Spectral Analysis

[19] Spectral analysis was utilized to examine periodicity of the proxy records. All records were detrended by subtracting the mean, and those that did not show a normal distribution were normalized

by calculating their log10 value. The variables examined were CaCO_3 , C/N ratio of organic matter, and oxygenation index (benthic factor 2).

[20] Spectral analysis was performed by the REDFIT procedure [*Schulz and Mudelsee, 2002*]

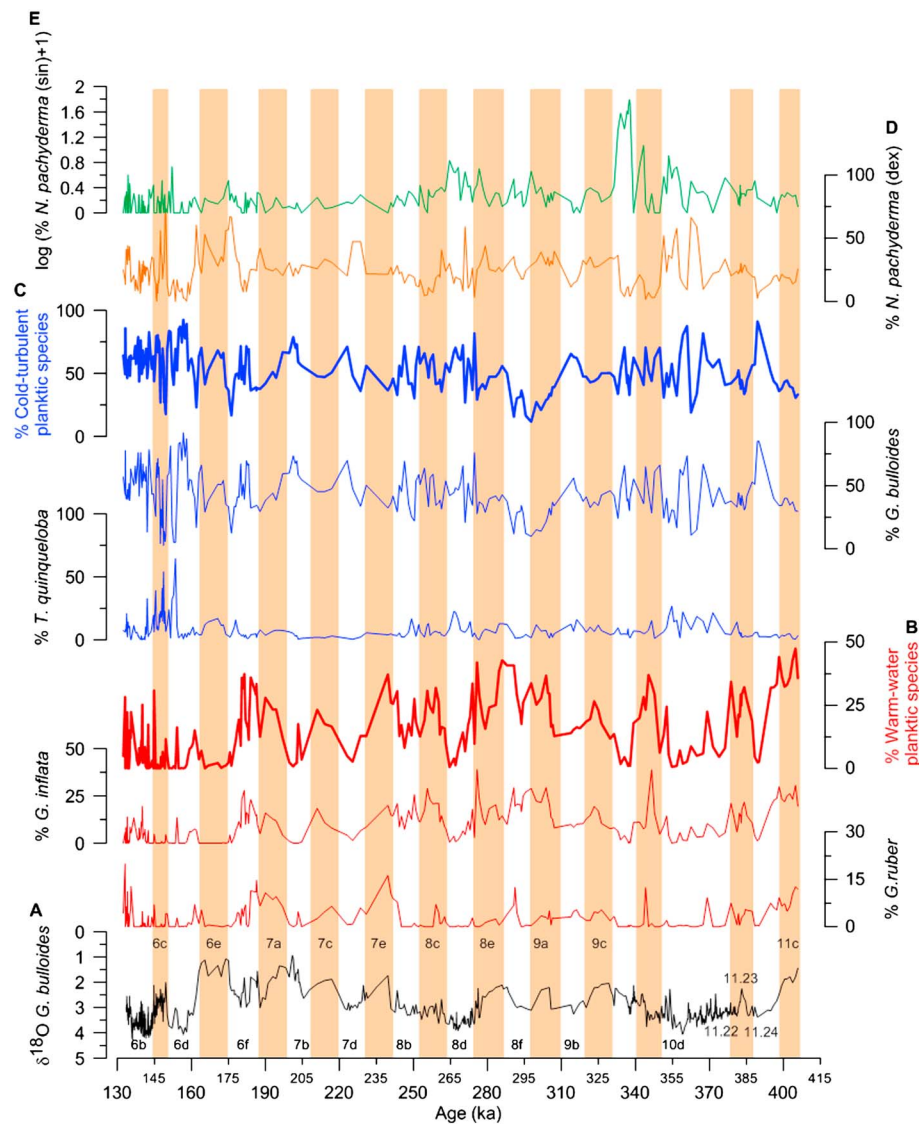


Figure 3. Planktic foraminiferal assemblages at PRGL1. A. *G. bulloides* $\delta^{18}\text{O}$ values. The values from 133 ka to 265 ka were taken from *Sierra et al.* [2009], while values from 266 ka to 406 ka were taken from *Frigola et al.* [2012]. B. Percent of warm-water species and its main contributors: *G. inflata* and *G. ruber*. C. Percent of cold-turbulent species and its two contributors: *G. bulloides* and *T. quinqueloba*. D. Percent of *N. pachyderma* (dex). E. $\log_{10} (\% N. pachyderma (\text{sin}) + 1)$. Orange bars represent warming events interpreted on the basis of $\delta^{18}\text{O}$ values of *G. bulloides* and % warm-water planktic species.

included in PAST 2.17b [Hammer et al., 2001]. This procedure uses a Lomb periodogram algorithm to calculate power spectral density. In order to reduce the noise, two equal segments were used and averaged to obtain the spectra. We also show 90% statistical significance of peaks based on a parametric approaching (Chi-squared distribution).

[21] Cross-coherence analysis was performed using the Welch method by means of MatLab. The method consists of dividing the time series data into segments, computing modified periodograms of each segment, and then averaging the power spectral density estimates [Welch, 1967]. We used two

segments (136 ka each); therefore, only periodicities less than 42 ka (three cycles/segment) could be studied. Coherence confidence levels were estimated according to *Amos and Koopmans* [1963] and phase uncertainty via Monte Carlo analysis.

4. Results

4.1. Benthic and Planktic Foraminifer Assemblages

[22] The results of the principal component analysis over the benthic foraminifer fauna are summarized

in Table 1 (present study). Three principal component factors were extracted, explaining a total variance of 81.2%. In order to provide climatic context, we compared the benthic assemblage data with the *G. bulloides* $\delta^{18}\text{O}$ record (Figure 2A)

[23] Factor 1, explaining 42.5% of the variance, is mainly composed by *Bulimina acueleata* / *Bulimina marginata*, *Cibicidoides pachyderma*, *Melonis*

barleeanus, *Bulimina inflata*, *Cassidulina laevigata*, and *Uvigerina peregrina*. This association preferentially dominated interglacial stages (Figure 2B). However, it was also found at the end of MIS 8.

[24] For factor 2 (18.1% of the variance), the main species are *Trifarina angulosa*, *Cassidulina laevigata*, *Quinqueloculina seminulum*, and *Pyrgo oblonga*. This assemblage was more characteristic

Table 2. Descriptive Statistics of the Percentages of the Elements Analyzed by Means of a PerkinElmer iCAP 6000 Inductively Coupled Plasma-Optical Emission Spectrometer. We Calculated Average, minimum, Maximum, and Standard Deviation

	Average	Minimum	Maximum	Std. Dev.
%Al	5.490	3.200	6.750	0.670
%Ca	10.670	7.320	14.940	1.400
%K	1.670	1.210	2.150	0.170
%Sr	0.035	0.028	0.044	0.003

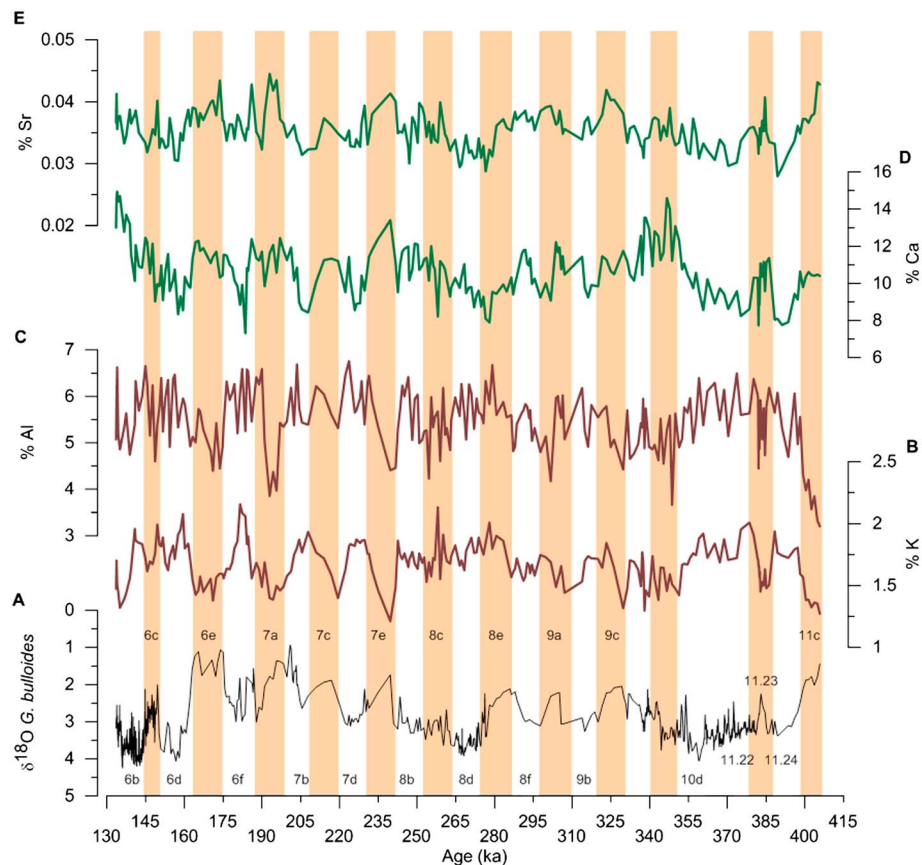


Figure 4. Elemental analysis at PRGL1. A. *G. bulloides* $\delta^{18}\text{O}$ values. The values from 133 ka to 265 ka were taken from *Sierro et al.* [2009], while values from 266 ka to 406 ka were taken from *Frigola et al.* [2012]. B. Percent of K. C. Percent of Al. D. Percent of Ca. E. Percent of Sr. Orange bars represent warming events interpreted on the basis of $\delta^{18}\text{O}$ values of *G. bulloides* and % warm-water planktic species.

of glacial stages and substages (Figure 2D). Compared with the other factors the duration of these events were shorter, commonly less than 5 ka.

[25] Factor 3, with an explained variance of 20.6%, is mainly comprised by *Bolivina dilatata* and in a lesser extent by *Bulimina aculeata* / *Bulimina marginata*. These species were more common

during glacial stages. Unlike the other two factors, it showed very low values and limited variability along MIS 7, 8, and 9 (Figure 2C).

[26] The planktic foraminifer assemblages were dominated by *Globigerina bulloides*, *Neogloboquadrina pachyderma* (dex), *Globorotalia inflata*, and in a lesser extent by *Globigerinoides ruber* (alba) and

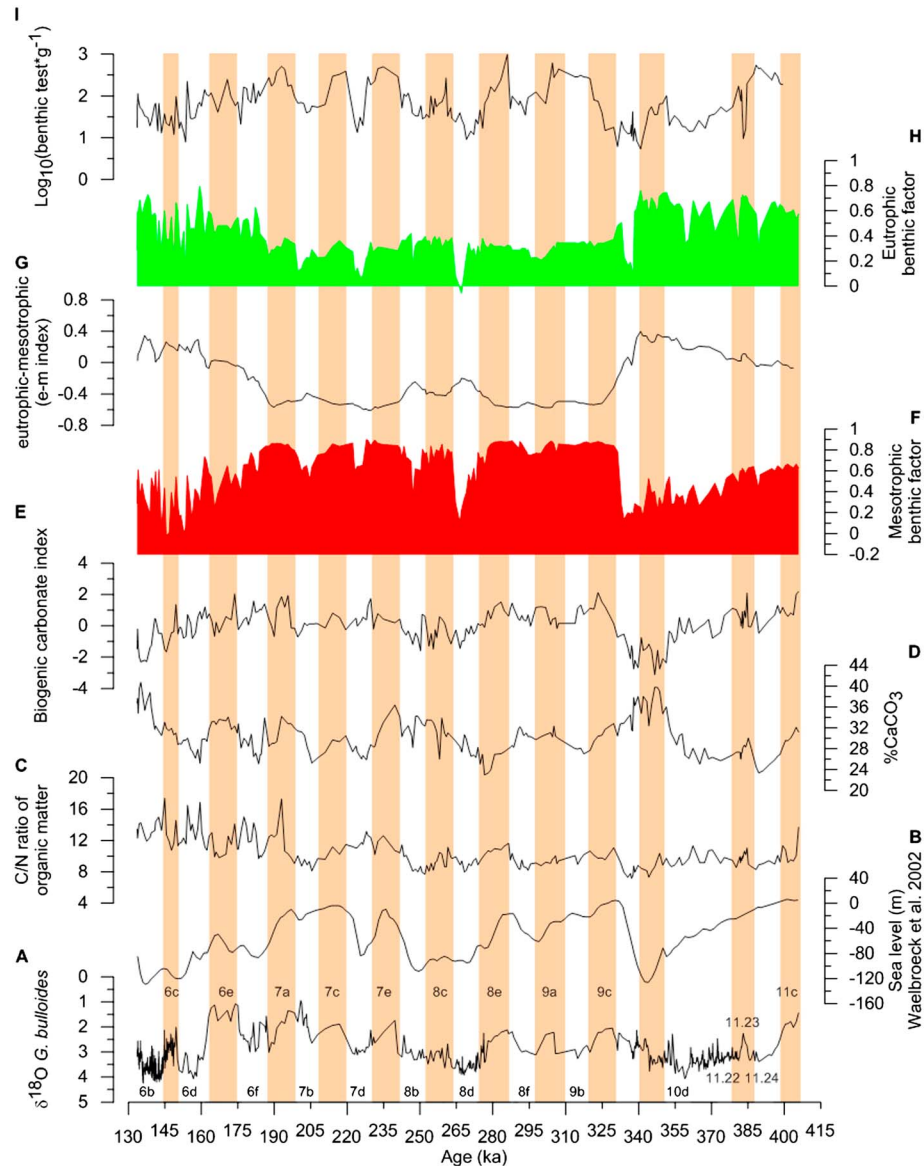


Figure 5. The effects of sea level changes on bottom conditions of the upper slope of the Gulf of Lions monitored by benthic foraminifer assemblages and geochemical proxies. A. *G. bulloides* $\delta^{18}\text{O}$ values. The values from 133 ka to 265 ka were taken from *Sierro et al.* [2009], while values from 266 ka to 406 ka were taken from *Frigola et al.* [2012]. B. Sea level reconstruction [*Waelbroeck et al.*, 2002]. C. C/N ratio of organic matter used as a proxy of its source from continental (high values) to marine (low values). D. Percent of CaCO_3 . E. Biogenic carbonate index used as a proxy of carbonate source, where low values indicate a detrital source and higher values a marine source. F. Loadings of the mesotrophic benthic factor. G. The difference between five points running average eutrophic and mesotrophic factors (e-m index). H. Loadings of the eutrophic benthic factor. I. Log₁₀ of benthic foraminifer tests per gram of dry sediment. Orange bars represent warming events interpreted on the basis of $\delta^{18}\text{O}$ values of *G. bulloides* and % warm-water planktic species.

Turborotalita quinqueloba (Figure 3). As in benthic foraminifer assemblages, we added the *G. bulloides* $\delta^{18}\text{O}$ record to provide climatic context to planktic foraminifer data (Figure 3A)

[27] In order to monitor the response of planktic foraminifers to thermal stratification of the water column, we calculated the relative proportion of warm-water planktic species. Based on a previous study in the Gulf of Lions by Cortina *et al.* [2011], we grouped *Globigerina Inflata* and *Globigerinoides ruber* (alba) as the main warm-water inhabiting species. Besides these two main species, *Globigerinella calida*, *Globigerinella digitata*, *Globigerinoides conglobatus*, *Globorotalia menardii*, *Globoturborotalita tenellus*, *Globoturborotalita rubescens*, *Neogloboquadrina dutertrei*, and *Orbulina universa* were also considered as warm-water species [Bé, 1977]. The percentage of warm-water planktic species usually increased during interglacial stages compared to glacial ones, largely in agreement with factor 1 (Figure 3B), but warm-water events were not limited to interglacial stages, since some warming events were also observed during glacial periods in which these species were abundant.

[28] Following results of Cortina *et al.* [2011] at the same core site, we considered *G. bulloides* and *T. quinqueloba* as species related with cold-turbulent environments in the water column, and *G. bulloides* linked with productivity events as well. The percentage of the cold-turbulent group peaked during glacial periods MIS 10, 8 and 6, and during glacial substages (Figure 3C), inversely to percentage of warm-water planktic species (Figures 3B and 3C).

[29] The warm-temperate species *N. pachyderma* (dex) showed an intermediate behavior between the warm-water and cold-turbulent groups and exhibited less variability than them. However, it dominated the planktic association in two periods: around 170 ka (6e) and 355 ka (Figure 3D).

[30] Although the polar species *N. pachyderma* (sin) dominated the planktic foraminifer assemblage (values about 50%) around 335 ka (Termination IV), they were typically less than 10% of the assemblage. Consequently, in order to interpret its variability, we represented $\log_{10} (\% \text{ N.pachyderma (sin)} + 1)$. Besides the 335 ka event, increases of this polar-adapted species were recorded during 8d and 10d (Figure 3E)

4.2. Geochemical Records

[31] Descriptive statistics of geochemical analyses are summarized in Table 2. Following the same procedure as in the micropaleontological assemblages, we compared the geochemical data to the *G. bulloides* $\delta^{18}\text{O}$ record (Figure 4A) to provide climatic context to geochemical data. Calcium was

the most abundant element, followed by Al, K, and Sr. Al and K showed similar trends, reaching maximum values around MIS 7 and the beginning of MIS 6 (6e) (Figures 4B and 4C). Calcium and Sr exhibit similar but inverse trends compared to elements related to silicate sources (i.e., Al, K) (Figures 4D and 4E).

[32] The C/N ratio is usually driven by the changing rates of supply of terrestrial versus marine organic matter to the sea floor. Values close to 5 are characteristic of a dominant marine source for the organic carbon, while values as high as 15 mainly reflect a terrestrial organic carbon source [Zeebe and Wolf-Gladrow, 2001]. The C/N ratio varied from 8 to 16. It reached higher values during MIS 6, but was generally lower during the rest of the record. It showed a long-term (low-frequency) variability in all marine isotopic stages, although oscillations were more pronounced during MIS 6 (Figure 5C).

[33] The CaCO_3 concentration (CHN analyzed) was highly variable at high and low frequencies but typically (see section 4.3) displayed elevated values at the end of glacial stages (MIS 6, 8, and 10) (Figure 5D). However, maximum values were also found during interglacial periods (e.g., 6e, 7a, 7e, 9c, 11c).

4.3. Spectral and Cross-spectral Analysis

[34] Power spectral analysis over all proxies revealed significant periodicities (90% confidence level) in the 41 ka and 19–23 ka band (Figure 6). The 19–23 ka precession-related cyclicity is clearly visible in the relative abundance of warm-water planktic species, *G. bulloides* $\delta^{18}\text{O}$ record, benthic factor 2, as well as in the relative percentages of Al, K, and Sr. Both precession and obliquity-related periodicity (41 ka) is seen in the C/N ratio of organic matter and the CaCO_3 record.

[35] Cross-spectral and phase analysis were performed to constrain the relationship between main periodicities of our proxies (Tables 3 and 4) (Annex 1, Annex 2). Coherences calculated were significant at 95% confidence level. In the frequency domain, we used phase values to determine whether two signals were in phase (values close to 0 degrees) or out of phase (values near +180 or –180 degrees). In the 19–23 ka band, coherence between *G. bulloides* $\delta^{18}\text{O}$ record and chemical records (Table 3) (Annex 1) show that lower isotopic values were consistently linked to high percentages of CaCO_3 and Sr. Higher isotopic values were associated with elevated percentages of Al and K. Coherence of the *G. bulloides* $\delta^{18}\text{O}$

All Supporting Information may be found in the online version of this article.

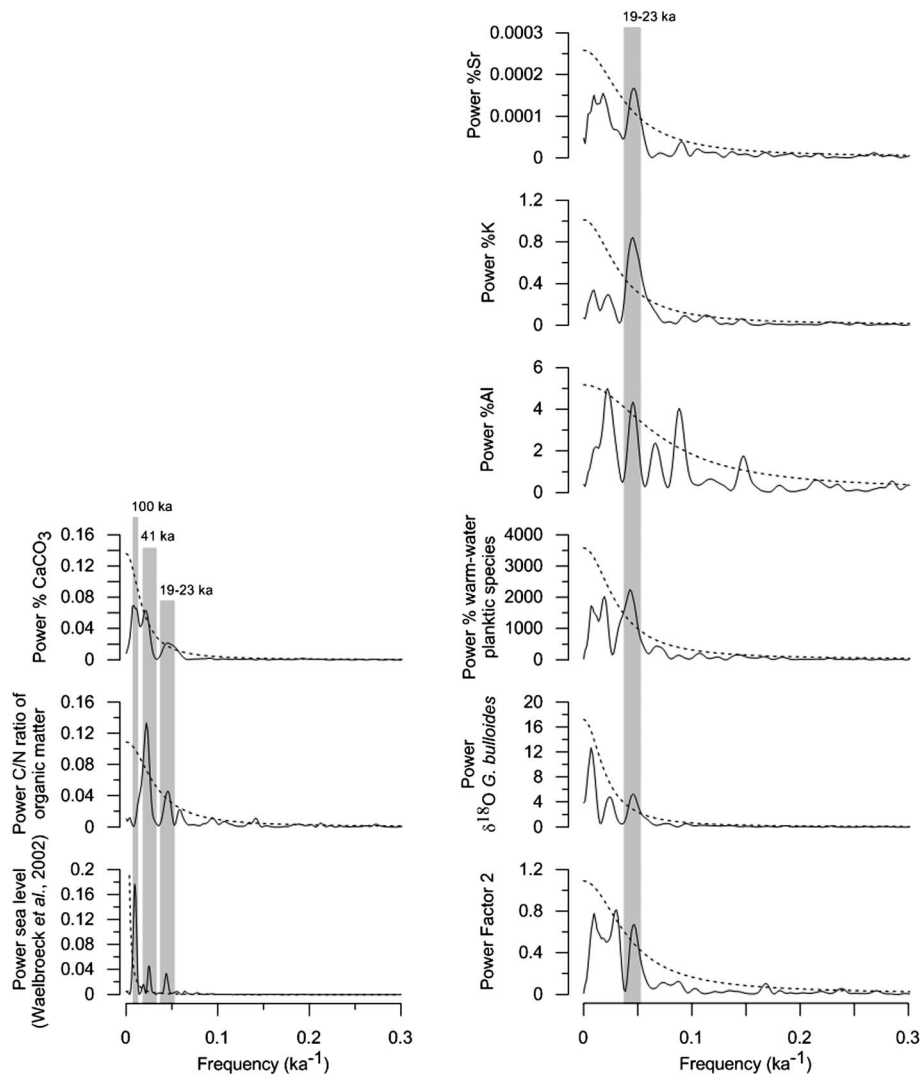


Figure 6. Spectral analysis. Power spectral analysis of variables performed by REDFIT procedure [Schulz and Mudelsee, 2002] included in PAST 2.17b [Hammer et al., 2001] using Lomb periodogram algorithm. Period of study was between 134 ka and 405 ka. For sea level reconstruction [Waelbroeck et al., 2002], we used all data available (0 to 429 ka). Dashed lines represent 90% statistical significance of peaks based on a parametric approaching (Chi-squared distribution). Gray bands represent main orbital bands centered at 19–23 ka, 41 ka and 100 ka periodicities.

record and biological proxies (Table 4) (Annex 2) shows a tight relationship between higher oxygen isotope data and high benthic factor 2 values, together with low C/N ratios and higher abundance of warm-water planktic species.

5. Discussion

5.1. Glacial-interglacial Changes in Bottom Conditions on the Upper Slope of the Gulf of Lions in Response to Sea Level and Climate Variability

[36] Changes in bottom sediments from the upper slope between 133 ka and 406 ka were the result

of the continuous interplay between sea level variations and climate variability, and their consequent impact on nutrient, organic matter, and detrital sediment inputs from the Rhone as well as vertical mixing of the water column, productivity, and bottom water ventilation.

5.1.1. Microfaunal Response to Environmental Changes

[37] As discussed by Cortina et al. [2011] at the same core site, benthic foraminifers reveal that bottom conditions from the Gulf of Lions varied from mesotrophic to eutrophic in response to changes in sea level and to ventilation of

Table 3. Cross-coherence and Phase Analysis at 19–23 ka Periodicity Of *G. bulloides* $\delta^{18}\text{O}$ Values and Bulk Sediment Analysis, Showing the Highest Coherence and its Phase in this Interval (19–23 ka Band). All Coherences Were Significant at 95% Confidence Level

Coherence (19–23 ka Band)					
Phase (19–23 ka Band)	$\delta^{18}\text{O}$ <i>G. bulloides</i>	% CaCO_3	%Sr	%Al	%K
$\delta^{18}\text{O}$ <i>G. bulloides</i>	1				
	0				
% CaCO_3	0.84	1			
	-155 ± 21	0			
%Sr	0.94	0.93	1		
	177 ± 21	-21 ± 20	0		
%Al	0.92	0.94	0.99	1	
	8 ± 19	175 ± 19	-166 ± 21	0	
%K	0.86	0.97	0.9	0.92	1
	34 ± 20	-174 ± 20	-151 ± 20	14 ± 20	0

Table 4. Cross-coherence and Phase Analysis at 19–23 ka Periodicity Of *G. bulloides* $\delta^{18}\text{O}$ Values and Biological Proxies, Showing the Highest Coherence and its Phase in This Interval (19–23 ka Band). All Coherences Were Significant at 95% Confidence Level

Coherence (19–23 ka Band)				
Phase (19–23 ka Band)	$\delta^{18}\text{O}$ <i>G. bulloides</i>	Factor 2	C/N	% Warm Planktic Species
$\delta^{18}\text{O}$ <i>G. bulloides</i>	1			
	0			
Factor 2	0.94	1		
	-2 ± 21	0		
C/N	0.98	0.99	1	
	-166 ± 20	-165 ± 19	0	
% Warm-water planktic species	0.89	0.95	0.92	1
	145 ± 20	145 ± 21	-50 ± 22	0

intermediate waters forced by variations in intensity of northwesterly winds. An extended discussion on the environmental conditions associated with each factor as a function of the habitat in which their main species live can be found in Cortina *et al.* [2011]. High concordance can be found between the benthic foraminifer species and factor analysis in this study and those found in [Cortina *et al.*, 2011] (Table 1) with the only exception of *B. aculeata* / *B. marginata* group because in the previous work, both species were counted separately. Summarizing, factor 1 is linked with mesotrophic and factor 3 with eutrophic conditions on the bottom. Factor 2 is related with oxygenated and turbulent bottom waters, so it can be used as bottom oxygenation index.

[38] The relative proportion of eutrophic (factor 3) and mesotrophic species (factor 1) mainly responded to changes in the rate of deliver of organic matter from river Rhone owing to sea level variability and its ensuing impact on the proximity of the river mouth to the upper slope [Cortina *et al.*, 2011]. During interglacial MIS 9 and 7,

benthic foraminifer assemblages were typically characteristic of mesotrophic conditions, with abundant factor 1 species such as *B. aculeata* / *B. marginata*, *C. pachyderma*, *M. barleeanus*, among others (Figure 2B). This assemblage is similar to that observed today in the upper slope [Fontanier *et al.*, 2008], an environment characterized by relatively high surface productivity and a prolonged season of summer stratification between April and November, which favors the development of microfauna characteristic of relatively low oxygen content in bottom waters and intermediate concentration of organic matter. Although phytoplankton growth is high in spring, the intensive winter ventilation leads to partial oxidation of the organic matter and the phytoplankton detritus sinking to the sea floor, preventing the development of carbon-rich, suboxic conditions at the bottom. These mesotrophic microfaunas were progressively replaced by eutrophic foraminifers, such as *B. dilatata* (factor 3) towards the glacial periods, especially in MIS10 and MIS 6 but less pronounced in MIS 8 (Figure 2C), probably in response to the higher organic carbon input from the river as the river mouth and prodelta deposits approached the shelf break.

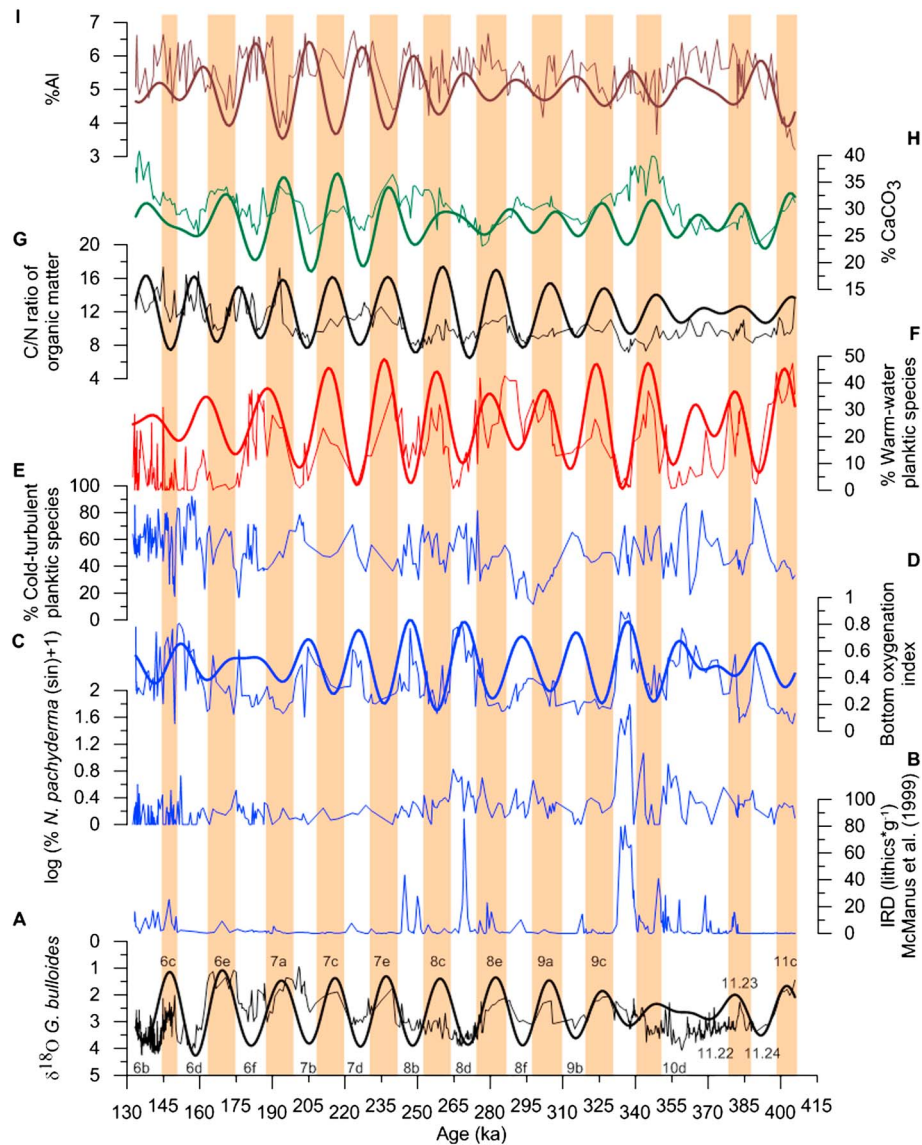


Figure 7. The effect of orbital precession over Gulf of Lions. A. *G. bulloides* $\delta^{18}\text{O}$ values. The values from 133 ka to 265 ka were taken from *Sierro et al.* [2009], while values from 266 ka to 406 ka were taken from *Frigola et al.* [2012]. B. IRD ($\text{lithics} \cdot \text{g}^{-1}$) from *McManus et al.* [1999]. C. $\text{Log}_{10} (\% N. pachyderma (\sin)+1)$. D. Bottom oxygenation index. E. Percent of cold-turbulent planktic species as indicators of turnover and mixing in the water column. F. Percent of warm-water planktic species as proxy of stratification of the water column. G. C/N ratio of organic matter used as a proxy of its source from continental (high values) to marine (low values). H. Percent of CaCO_3 . I. Percent of Al used as a proxy of silicate-related minerals since it is present in all aluminosilicates. Orange bars represent warming events interpreted on the basis of $\delta^{18}\text{O}$ values of *G. bulloides* and % warm-water planktic species. Thick line over the proxies represent Gaussian filter centered at 21 ka (e.g., 0.04687 ka^{-1}) performed with Analyseries 2.0. Gaussian filter only was performed over proxies with significant spectral peak at 19–23 ka band.

[39] The loadings of mesotrophic and eutrophic factors and especially the difference between the eutrophic-mesotrophic loadings (e-m index) (Figure 5G) was mainly driven by sea level changes, as shown by the similarity between this proxy and the global sea level record (Figure 5B). Three sequences of increasing e-m values were recorded in response to sea level variations related to glacial-interglacial 100 ka cycles between MIS11–10, MIS9–8, and MIS7–6 with

maximum values of e-m during glacial stages 10, 8, and 6. The lower e-m values at the end of MIS 8 compared to those of MIS 6 and 10 suggest a lower sea level fall monitored in the Gulf of Lions during this glacial period.

[40] MIS 11 is a particular interesting interglacial interval, during which even though high sea level and mesotrophic conditions persisted, some degree

of dysoxia prevailed as monitored by factor 3 (*B. dilatata*) (Figures 2C and 5H). Given the low input from the Rhone compared to glacial stages, these eutrophic conditions can be linked to either elevated productivity or reduced bottom ventilation. Taking into consideration the high values of warm-water planktic species during MIS 11 (Figure 3B) and the low percent values (except for substage 11.24) of the high-productive species *G. bulloides* (Figure 3C), the most plausible explanation is a drop in winter ventilation. Therefore, less frequent incursions of polar air masses during milder winters may be the principal cause of the appearance of *B. dilatata* during interglacial MIS 11.

5.1.2. Sedimentary Response to Environmental Changes

[41] Sediments deposited in the entire Gulf of Lions are mainly originated from the Rhone watershed, with a lower influence of Pyrenean rivers [Révillon *et al.*, 2011]. Although the Rhone river watershed is lithologically complex, the hydrographic basin is characterized by mountain catchments in the Alps consisting mainly of calcareous rocks [Ollivier *et al.*, 2010], in contrast with silicate-related Pyrenean catchments. For this reason, detrital carbonate is more linked to Rhone detrital input, while other elements, such as Al and K can be supplied by either the Rhone or the Pyrenean rivers. In consequence, changes in percentage of major elements in the Gulf of Lions should reflect the continuously changing input rates of detrital carbonate mainly supplied by the Rhone, biogenic calcite produced in the basin, and silicate-related detrital sediments supplied by the Rhone and the Pyrenean rivers. Hence, changes in sediment properties through time may provide the key to what controls sedimentation in the Gulf of Lions.

[42] Spectral analysis of the calcium carbonate record shows three main frequencies centered at 100 ka, 41 ka, and 19–23 ka bands (Figure 6). Although the 100 ka periodicity is not statistically significant owing to the length of the segments used in spectral analysis (136 ka), the importance of 100 ka and 41 ka periodicities, also evident in the spectral analysis of eustatic sea level records (Figure 6) (performed over the last 430 ka), supports the strong relationship between input of detrital carbonate and global sea level change. Calcium carbonate at PRGL1 reached maximum values at times of the lowest sea level, especially in glacial stages MIS10 and 6, and in a lesser extent

in MIS 8. In contrast, lower carbonate contents were observed during interglacial stages MIS11, 9, and 7 (Figure 5D). Similar to the e-m record, three sequences of long-term increase in calcium carbonate are associated with the 100 ka cycle of sea level, between MIS11–10, MIS 9–8, and MIS 7–6. These three sequences are also seen in the biogenic carbonate index (Figure 5E), indicating that the higher carbonate values found at times of lowest sea level are of detrital origin (high Sr content is typically related to productivity and biogenic calcite) [Claude and Hamelin, 2007]. In addition, the low numbers of benthic foraminifer tests per gram of sediment in glacial stages (Figure 5I) also confirms the low relative proportion of biogenic calcite at these stages. This indicates that an important component of the calcium carbonate is of detrital origin. These results (e-m index, biogenic carbonate index, benthic foraminifer test per gram) support the lower sea level drop monitored in the Gulf of Lions during MIS 8 compared to MIS 6 and 10 in agreement with the global sea level curve [Waelbroeck *et al.*, 2002] (Figure 5B).

[43] Although sea level seems to be the main forcing governing sediment composition on the upper slope of the Gulf of Lions, climate also can affect it by means of the amount of carbonate erosion in the catchment area of the Rhone as demonstrated by Ollivier *et al.* [2010]. This three-year survey study monitored an increasing proportion of carbonates during the flood events both in the solid and dissolved phases. However, based on the results discussed previously, these influences seem to be minor compared to that of sea level change.

[44] Similarly, the obliquity (41 ka) response of the CaCO₃ content and the C/N ratio of organic matter (Figure 6) should also be chiefly related to sea level oscillations. As stated before, C/N ratio varies in response to changes of the dominant source of organic matter from marine (low values) to terrestrial (high values). Alternatively, it has been demonstrated that aquatic organic matter is preferentially remineralized during sinking and at the sediment water boundary [Prahll *et al.*, 1980], and hence differential organic matter preservation at times of higher and lower burial rates can be invoked to explain in part changes in the C/N ratio. The higher values in MIS 6 were unambiguously related with maximum input of organic matter transported by the Rhone (Figure 5C). However, from MIS 7 to MIS 11, C/N values were lower during glacial stages when a higher input of terrestrial organic matter is expected and higher in interglacials when a lower input of terrestrial carbon is expected. This

can only be explained by changes in primary productivity or differential preservation. The occurrence of eutrophic conditions in the sea floor (Figure 5H) together with the high proportions of *G. bulloides* or *N. pachyderma* (dex) during glacial stages (Figures 3C and 3D), typically linked to high productivity, is consistent with the hypothesis of higher primary productivity during glacial stages. The higher flux of marine organic matter to the sea floor at these times may balance the higher input of terrestrial organic compounds, resulting in lower C/N values. Additionally, the high amplitude change in sedimentation rates between glacial and interglacial intervals may have played a significant role on organic matter preservation in the sediments. During highstands, the reduced sediment input from the river led to the formation of various condensed layers (Cl's) in the sediments [Sierra *et al.*, 2009], characterized by high amount of biogenic CaCO₃ associated among other biogenic sources with high content of benthic and planktic foraminifers (Figure 5I). These very low burial rates resulted in extended periods of organic matter degradation at the reactive sediment-water interface. These long periods of degradation probably favored the preservation of more refractory and more carbon-rich organic matter in the sediments. For this reason, biogenic CaCO₃ and C/N ratio reached maximum values in the obliquity band (41 ka) at times of higher sea level periods (7a, 7e, 8e, 9c, 11c) (Figures 5C and 5D)

5.2. Precession-Driven Changes in Bottom Water Ventilation and Sedimentation Processes in the Upper Slope of the Gulf of Lions

[45] Sea level variability is the main mechanism that controls environmental conditions on the seafloor in the upper slope of the Gulf of Lions. However, power in the precession band (19–23 ka) is also present in most of the proxies studied here, including the bottom oxygenation index (benthic factor 2), silicate-related sediment compounds (Al, K), Sr, warm-water planktic species, C/N ratio, and CaCO₃ (Figure 6). The combined effect of changes in river supply between high and low sea levels and the intensification or reduction of the northwesterlies forced by precession maxima and minima, respectively, appear to drive this variability.

[46] Cross-coherence (95% confidence interval) and phase analysis on the precession band (Tables 3 and 4) revealed a significant relationship between high *G. bulloides* $\delta^{18}\text{O}$ values and increases in silicate-related minerals (Al, K), bottom oxygenation index, and the input of fresh marine organic

matter (low C/N ratio). In contrast, low *G. bulloides* $\delta^{18}\text{O}$ values were linked to high abundance of warm-water planktic species, CaCO₃ and Sr.

[47] Figure 7 shows the orbital effect of precession over the Gulf of Lions. Proxies with significant precessional power (Figure 6) were also filtered at 19–23 ka band and the filter output represented by thicker lines. On the basis of this filter output, we related low *G. bulloides* $\delta^{18}\text{O}$ values (Figure 7A) to precession minima and high *G. bulloides* $\delta^{18}\text{O}$ values to precession maxima, assuming during this period an average lag of 4.8 ka between insolation forcing and $\delta^{18}\text{O}$ response at this band [Lisiecki and Raymo, 2005].

[48] Oscillations of sea surface temperature at the precession band were recorded by changes in percentage of the warm-water planktic species throughout the record (Figure 7F). Only towards the end of MIS 6 is variability in the precession band overprinted by millennial-scale oscillations [Cortina *et al.*, 2011]. At the precession band, high values of warm-water planktic species coincided with intervals of low *G. bulloides* $\delta^{18}\text{O}$ values (Coherence = 0.89) (Table 4) (Figure 7A.), indicating that warmer conditions were reached in the water column of the Gulf of Lions during precession minima. Although this general model can generally be applied throughout the entire record, an exception occurs at around 170 ka, coinciding with deposition of Sapropel 6 in the eastern Mediterranean Sea (MIS 6.e) [Calvert and Fontugne, 2001]. No increase in warm-water planktic foraminifers was seen in this interval of high summer insolation. Instead, high percentages of *N. pachyderma* were recognized (Figure 3D). The relatively high abundance of *N. pachyderma* (dex.) is linked to increased annual stratification in the water column, leading to the formation of a deep chlorophyll maximum. Although alkenone-based analysis indicates a higher temperature during this interval (unpublished data), these extremely low $\delta^{18}\text{O}$ values can be interpreted as evidence for a strong influence of isotopically light freshwater [Williams *et al.*, 1978; Fontugne *et al.*, 1989; Tang and Stott, 1993] that favored stratification. Although no sapropel was deposited in the Gulf of Lions, prominent minima in planktic $\delta^{18}\text{O}$ values throughout the last 2.8 Myr in the Mediterranean have been related to sapropel deposition and enhanced freshwater discharge of circum-Mediterranean climate [Rossignol-Strick, 1983; Lourens *et al.*, 1992]. Sapropel S6 was deposited during a glacial period, although increased rainfall has been reported both in the eastern [Ayalon *et al.*, 2002] and western basins [Plagnes *et al.*, 2002] that favored the growth of *N. pachyderma* (dex) at the expense of the characteristic warm-water planktic species (*G. ruber* and *G. inflata*) (Figures 3B and 3D).

[49] Furthermore, in the precession band, high *G. bulloides* $\delta^{18}\text{O}$ values were related to enhanced



bottom ventilation (bottom oxygenation index) (Coherence = 0.94) (Figures 7A and 7D). Our results suggest a variation of the intensity of northwesterly winds at the precession band as the main mechanism driving intermediate-water ventilation in the Gulf of Lions. During glacial substages, reinforcement of northwesterly winds as a result of polar air incursions [Cacho *et al.*, 2000; Moreno *et al.*, 2002; Sierro *et al.*, 2005] intensified vertical convection and mixing, promoting bottom ventilation (high bottom oxygenation index) (Figure 7D) and a reduction of warm-water planktic foraminifers typically associated to summer thermal stratification (Figure 7F). This intense convection brought nutrients to surface waters, enhancing primary productivity (low C/N ratio) (Figure 7G). Moreover, lowered sea levels allowed nutrient input from the Rhone and Pyreneans rivers to somewhat circumvent estuarine and shelf environments, discharging instead more directly into the open ocean, and thus spurring enhanced primary productivity. Although the percentage of cold-turbulent planktic species did not show a 19–23 ka periodicity, they peaked at times of precession maxima (Figure 7E), supporting the relationship between higher overturning and productivity during cold substages and precession maxima. The two exceptions to these precessionally driven changes in bottom ventilation occurred during MIS 9.b, where an enhanced bottom ventilation was not recorded, and at the end of MIS 6, where millennial-scale oscillations replaced precessional forcing. The enhancement of bottom oxygenation at millennial scale during the end of MIS 6 could be the result of the amplification of this signal during lowstands due to the shallower water column at site PRGL1. Based on C/N ratios, the lowest sea level values (highest C/N ratios) were recorded in this interval (Figure 7G). These lowest sea levels could favor ventilation events modulated at high climatic frequencies.

[50] At the precession band, the two strongest events of bottom ventilation in the Gulf Lions were recorded at around 335 ka (Termination IV) and during stage 8e (Figure 7D); these intervals are coincident with the two IRD-rich layers recorded in the North Atlantic by *McManus et al.* [1999] (Figure 7B). These two periods reflected an increase of the polar species *N. pachyderma* (sin) (Figure 7C) present in the Mediterranean during extreme cold periods like in Heinrich events [Rohling *et al.*, 1998; Sierro *et al.*, 2005]. We interpret these results as a climatic teleconnection between high and low latitudes. Maximum IRD discharge, related to maximum cooling of North Atlantic surface waters, correlates with intensification of northwesterly winds [Cacho *et al.*, 2000; Moreno *et al.*, 2002;

Sierro et al., 2005] and maximum bottom ventilation (bottom oxygenation index). This model is in agreement with that proposed by *Rohling et al.* [1998].

[51] These events of ventilation took place at water depths similar to those of WIW formation (about 200 meters). Therefore, our data suggest an intensification of WIW, and consequently its contribution to Mediterranean Outflow Waters (MOW), at times of precession maxima. Moreover, although the formation of WIW and WMDW occur at different places, northwesterly winds are the main forcing that governs them. Hence, the intensification of northwesterly winds at times of precession maxima from MIS 7 to 11 could be driving variability in WMDW formation.

[52] Although eustatic changes are mainly driven by variations in Earth's obliquity and the 100 ka cycle, precession oscillations also played a significant role on ice-sheet dynamics and sea level, as observed in spectral analysis of sea level reconstruction [Waelbroeck *et al.*, 2002] (Figure 6). Site PRGL1 is located towards the southmost part of the Gulf of Lions and therefore closer to the influence of the Pyrenean rivers (e.g., Aude, Têt, Agly). Indeed, glacial paleopath of these rivers have been identified on the shelf close to PRGL1 (Figure 1). In the precession band, the highstand periods during the interglacial substages (low *G. bulloides* $\delta^{18}\text{O}$ values) (Figure 7A) were typically characterized by abundant warm-water planktic foraminifers (Figure 7F) and Cl's formation [Sierro *et al.*, 2009] rich in biogenic carbonate (Figure 7H) and Sr as revealed by cross-coherence analysis (Tables 3 and 4). These beds, linked to precession minima, were replaced by sediments more enriched in silicate-derived elements (Al, K) due to the proximity of the mouths of Pyrenean rivers as sea level dropped in response to increasing precession and lower boreal summer insolation (Figure 7I)(Table 3). During glacial stages MIS 6, 8, and 10, and especially at times of glacial maxima when the sea level drop was more pronounced and the coastline approached the shelf break, the influence of the Rhone supply increased. Consequently, CaCO_3 derived from the Alps watershed dominated, diluting the relative contribution of the silicate-rich sediments supplied by the Pyrenean rivers and the biogenic carbonate produced in the basin.

6. Conclusions

[53] Bottom conditions in the upper slope of the Gulf of Lions from MIS 6 to 11 varied at different time scales as a consequence of changes in sea level, particularly driven by ice-sheet dynamics at 100 ka and 41 ka bands and in a lesser extent at

19–23 ka band. Moreover, the intensity of the northwesterly winds driven by precession also influenced these bottom environments.

[54] Benthic foraminifer assemblages changed from mesotrophic to eutrophic as sea level dropped during glacial periods and the Rhone prodelta approached the shelf break. A similar change was recorded in the carbonate content of the sediments, which reached maximum values during glacial periods of MIS 6, 8, and 10. A seaward migration of the Rhone prodelta during these stages increased the supply of detrital carbonate mainly originated in the Alps catchments. The coincidence of high carbonate with the proximity of the Rhone delta strongly supports a dominant detrital source for carbonate during glacial periods. Moreover, these records reveal a lower sea level fall monitored in the Gulf of Lions in the MIS 8, compared to MIS 6 and 10. In contrast, during interglacial stages typically linked to high sea levels and highstands, biogenic CaCO_3 from calcareous shells and other biogenic debris was the main source of carbonate.

[55] Precession-driven incursions of northwesterly winds during precession maxima were clearly recorded in the Gulf of Lions record. These cold-air incursions to the NW Mediterranean lowered sea surface temperature and caused both, the enhancement of marine productivity (low C/N) and the ventilation of bottom waters (high bottom oxygenation index). During interglacial periods, especially in MIS7 and 9, these intervals of minimum insolation were usually associated with lower sea levels and consequently with relatively higher silicate-related elements due to the larger influence of Pyrenees rivers. This influence, however, was diluted by the Rhone discharge (high detrital CaCO_3 content) during the lowest sea level periods, which are more linked to 100 ka periods.

[56] The incursions of northwesterly winds should increase WIW formation and consequently its contribution to MOW at times of precession maxima. However, because ventilation of the upper slope depends on WIW formation and changes of water depth through time, the relationship between bottom oxygenation and enhanced northwesterly winds can be amplified during periods of lowstands. Moreover, as northwesterly winds govern both the WIW and WMDW formation, precession could be involved in WMDW formation from MIS 7 to 11.

Acknowledgments

[57] This work was funded by the Spanish “Ministerio de Ciencia e Innovación” MICINN project CGL2011-26493 and GRACCIE (CONSOLIDER-INGENIO CSD 2007–00067), the regional government of Castilla y León project GR34, and by a MEC FPI Grant (BES-2007-17602) awarded to Aleix Cortina. Two anonymous reviewers are greatly acknowledged for their comments that contributed to improve the final version of this manuscript.

References

- Aloisi, J. C. (1986), Sur un modèle de sédimentation deltaïque: contribution à la connaissance des marges passives, 162 pp., Université de Perpignan, Perpignan.
- Amos, D., and L. H. Koopmans (1963), Tables of the distribution of the coefficient of coherence for stationary bivariate gaussian processes, Sandia Corporation, available from the Office of Technical Services, Dept. of Commerce, Washington, DC.
- Ayalon, A., M. Bar-Matthews, and A. Kaufman (2002), Climatic conditions during marine oxygen isotope stage 6 in the eastern Mediterranean region from the isotopic composition of speleothems of Soreq Cave, Israel, *Geology*, 30(4), 303–306.
- Bé, A. W. H. (1977), An ecological, zoogeographic and taxonomic review of recent planktonic foraminifera, in *Oceanic Micropaleontology*, edited by A. T. S. Ramsay, pp. 1–100, Academic Press, London.
- Béthoux, J. P., X. D. de Madron, F. Nyffeler, and D. Tailliez (2002), Deep water in the western Mediterranean: peculiar 1999 and 2000 characteristics, shelf formation hypothesis, variability since 1970 and geochemical inferences, *J. Marine Syst.*, 33, 117–131.
- Cacho, I., J. O. Grimalt, F. J. Sierro, N. Shackleton, and M. Canals (2000), Evidence for enhanced Mediterranean thermohaline circulation during rapid climatic coolings, *Earth Planet. Sci. Lett.*, 183(3–4), 417–429.
- Calvert, S. E., and M. R. Fontugne (2001), On the late Pleistocene–Holocene sapropel record of climatic and oceanographic variability in the eastern Mediterranean, *Paleoceanography*, 16(1), 78–94.
- Canals, M., P. Puig, X. D. De Madron, S. Heussner, A. Palanques, and J. Fabres (2006), Flushing submarine canyons, *Nature*, 444(7117), 354–357.
- Claude, C., and B. Hamelin (2007), Isotopic tracers of water masses and deep currents, in Proxies in Late Cenozoic Paleoclimatology, edited by C. Hillaire-Marcel and A. De Vernal, pp. 567–635, Elsevier, Amsterdam.
- Cortina, A., F. J. Sierro, B. González-Mora, A. Asioli, and J. A. Flores (2011), Impact of climate and sea level changes on the ventilation of intermediate water and benthic foraminifer assemblages in the Gulf of Lions, off South France, during MIS 6 and 7, *Palaeoogeogr. Palaeoecol.*, 309(3–4), 215–228.
- Dufau-Julliand, C., P. Marsaleix, A. Petrenko, and I. Dekeyser (2004), Three-dimensional modeling of the Gulf of Lion’s hydrodynamics (northwest Mediterranean) during January 1999 (MOOGLI3 Experiment) and late winter 1999: Western Mediterranean Intermediate Water’s (WIW’s) formation and its cascading over the shelf break, *J. Geophys. Res.*, 109, C11002, doi:10.1029/2003JC002019.

- Ellis and Messina (2007), Ellis and Messina Catalogue of Foraminifera, Micropaleontology Press, New York.
- Fatela, F., and R. Taborda (2002), Confidence limits of species proportions in microfossil assemblages, *Mar. Micropaleontol.*, *45*(2), 169–174.
- Filipsson, H. L., J. M. Bernhard, S. A. Lincoln, and D. C. McCorkle (2010), A culture-based calibration of benthic foraminiferal paleotemperature proxies: $\delta^{18}O$ and Mg/Ca results, *Biogeosciences*, *7*(4), 1335–1347.
- Fontanier, C., et al. (2008), Live foraminifera from the open slope between Grand Rhone and Petit Rhone Canyons (Gulf of Lions, NW Mediterranean), *Deep-Sea Res. Pt. I*, *55*(11), 1532–1553.
- Fontugne, M. R., M. Paterne, S. E. Calvert, A. Murat, F. Guichard, and M. Arnold (1989), Adriatic deep water formation during the Holocene: Implication for the reoxygenation of the deep eastern Mediterranean Sea, *Paleoceanography*, *4*(2), 199–206.
- Frigola, J., A. Moreno, I. Cacho, M. Canals, F. J. Sierro, J. A. Flores, and J. O. Grimalt (2008), Evidence of abrupt changes in Western Mediterranean Deep Water circulation during the last 50 ka: A high-resolution marine record from the Balearic Sea, *Quatern. Int.*, *181*(1), 88–104.
- Frigola, J., et al. (2012), A 500 kyr record of global sea-level oscillations in the Gulf of Lion, Mediterranean Sea: new insights into MIS 3 sea-level variability, *Clim. Past*, *8*(3), 1067–1077.
- Gaudin, M., S. Berne, J. M. Jouanneau, A. Palanques, P. Puig, T. Mulder, P. Cirac, M. Rabineau, and P. Imbert (2006), Massive sand beds attributed to deposition by dense water cascades in the Bourcart canyon head, Gulf of Lions (northwestern Mediterranean Sea), *Mar. Geol.*, *234*(1–4), 111–128.
- Hammer, Ø., D. A. T. Harper, and P. D. Ryan (2001), Past: Paleontological Statistics Software Package for Education and Data Analysis, *Palaeontologia Electronica*, *4*(1), art 4: 9 pp.
- Hemleben, C., M. Spindler, and O. R. Anderson (1989), *Modern Planktonic Foraminifera*, 363 pp., Springer, New York.
- Jorissen, F. J. (1987), The distribution of benthic foraminifera in the Adriatic Sea, *Mar. Micropaleontol.*, *12*(C), 21–48.
- Jouet, G., S. Berné, M. Rabineau, M. A. Bassetti, P. Bernier, B. Dennielou, F. J. Sierro, J. A. Flores, and M. Taviani (2006), Shoreface migrations at the shelf edge and sea-level changes around the Last Glacial Maximum (Gulf of Lions, NW Mediterranean), *Mar. Geol.*, *234*(1–4), 21–42.
- Kennedy, P., H. Kennedy, and S. Papadimitriou (2005), The effect of acidification on the determination of organic carbon, total nitrogen and their stable isotopic composition in algae and marine sediment, *Rapid Commun. Mass Sp.*, *19*(8), 1063–1068.
- Lefèvre, D., H. J. Minas, M. Minas, C. Robinson, P. J. L. Williams, and E. M. S. Woodward (1997), Review of gross community production, primary production, net community production and dark community respiration in the Gulf of Lions, *Deep-Sea Res. Pt. II*, *44*(3–4), 801–832.
- Lisiecki, L. E., and M. E. Raymo (2005), A Pliocene-Pleistocene stack of 57 globally distributed benthic $\delta^{18}O$ records, *Paleoceanography*, *20*(1), PA1003.
- Loeblich, A. R., and H. Tappan (1988), *Foraminiferal Genera and Their Classification*, 1728 pp., Springer, New York.
- Lourens, L. J., F. J. Hilgen, L. Gudjonsson, and W. J. Zachariasse (1992), Late Pliocene to early Pleistocene astronomically forced sea surface productivity and temperature variations in the Mediterranean, *Mar. Micropaleontol.*, *19*(1–2), 49–78.
- McManus, J. F., D. W. Oppo, and J. L. Cullen (1999), A 0.5-million-year record of millennial-scale climate variability in the North Atlantic, *Science*, *283*(5404), 971–975.
- Millot, C. (1990), The Gulf of Lions' hydrodynamics, *Cont. Shelf Res.*, *10*(9–11), 885–894.
- Millot, C. (1999), Circulation in the Western Mediterranean Sea, *J. Marine Syst.*, *20*(1–4), 423–442.
- Moreno, A., I. Cacho, M. Canals, M. A. Prins, M. F. Sánchez-Goñi, J. O. Grimalt, and G. J. Weltje (2002), Saharan dust transport and high-latitude glacial climatic variability: The Alboran Sea record, *Quaternary Res.*, *58*(3), 318–328.
- Ollivier, P., B. Hamelin, and O. Radakovitch (2010), Seasonal variations of physical and chemical erosion: A three-year survey of the Rhone River (France), *Geochim. Cosmochim. Ac.*, *74*(3), 907–927.
- Palanques, A., X. Durrieu de Madron, P. Puig, J. Fabres, J. Guillén, A. Calafat, M. Canals, S. Heussner, and J. m. Bonnin (2006), Suspended sediment fluxes and transport processes in the Gulf of Lions submarine canyons. The role of storms and dense water cascading, *Mar. Geol.*, *234*(1–4), 43–61.
- Plagnes, V., C. Causse, G. Dominique, M. Paterne, and D. Blamart (2002), A discontinuous climatic record from 187 to 74 ka from a speleothem of the Clamouse Cave (south of France), *Earth Planet. Sci. Lett.*, *201*(1), 87–103.
- Prahl, F. G., J. T. Bennett, and R. Carpenter (1980), The early diagenesis of aliphatic hydrocarbons and organic matter in sedimentary particulates from Dabob Bay, Washington, *Geochim. Cosmochim. Ac.*, *44*(12), 1967–1976.
- Révillon, S., G. Jouet, G. Bayon, M. Rabineau, B. Dennielou, C. Hémond, and S. Berné (2011), The provenance of sediments in the Gulf of Lions, western Mediterranean Sea, *Geochem. Geophys. Geosyst.*, *12*(8), Q08006.
- Rohling, E. J., A. Hayes, S. De Rijk, D. Kroon, W. J. Zachariasse, and D. Eisma (1998), Abrupt cold spells in the northwest Mediterranean, *Paleoceanography*, *13*(4), 316–322.
- Rossignol-Strick, M. (1983), African monsoons, an immediate climate response to orbital insolation, *Nature*, *304*(5921), 46–49.
- Schulz, M., and M. Mudelsee (2002), REDFIT: Estimating red-noise spectra directly from unevenly spaced paleoclimatic time series, *Comput. Geosci.*, *28*(3), 421–426.
- Sierro, F. J., et al. (2005), Impact of iceberg melting on Mediterranean thermohaline circulation during Heinrich events, *Paleoceanography*, *20*(2), PA2019.
- Sierro, F. J., et al. (2009), Phase relationship between sea level and abrupt climate change, *Quaternary Sci. Rev.*, *28*(25–26), 2867–2881.
- Tang, C. M., and L. D. Stott (1993), Seasonal salinity changes during Mediterranean sapropel deposition 9000 years B.P.; Evidence from isotopic analyses of individual planktonic foraminifera, *Paleoceanography*, *8*(4), 473–493.
- Van Iperen, J., and W. Helder (1985), A method for the determination of organic carbon in calcareous marine sediments, *Mar. Geol.*, *64*, 179–187.
- Waelbroeck, C., L. Labeyrie, E. Michel, J. C. Duplessy, J. F. McManus, K. Lambeck, E. Balbon, and M. Labracherie (2002), Sea-level and deep water temperature changes derived from benthic foraminifera isotopic records, *Quaternary Sci. Rev.*, *21*(1–3), 295–305.



Welch, P. D. (1967), The use of fast Fourier transform for the estimation of power spectra: A method based on time averaging over short, modified periodograms, *Audio and Electroacoustics, IEEE Transactions on*, 15(2), 70–73.

Williams, D. F., R. C. Thunell, and J. P. Kennett (1978), Periodic freshwater flooding and stagnation of the

eastern mediterranean sea during the late quaternary, *Science*, 201(4352), 252–254.

Zeebe, R., and D. Wolf-Gladrow (2001), CO₂ in seawater: Equilibrium, kinetics, isotopes, edited, p. 346, Elsevier Oceanography Series, Elsevier, Amsterdam.